Performance Analysis of Standalone UWB Positioning Inside Forest Canopy

Zuoya Liu, Harri Kaartinen, Teemu Hakala, Juha Hyyppä, Antero Kukko, and Ruizhi Chen

***Abstract*— A precise and reliable 2-D/3-D positioning solution is a significant advancement for robotics-assisted surveying in forestry automation. Ultrawideband (UWB) positioning, an outstanding technology for high accuracy and high robustness positioning solutions, has emerged as the most promising candidate to serve this application. It has the potential to reduce the meter-level positioning accuracy of the global navigation satellite system (GNSS) inside forest canopies down to the decimeter level independent of other sensors/measurements. However, to date, little is known about the actual performance of standalone UWB positioning in these environments. In this article, a detailed performance analysis of a standalone UWB positioning system in a GNSS-denied forest environment with slight and serious non-line-of-sight (NLOS) propagations was performed. Positioning accuracy and the effect of the positioning update rate on the accuracy, as well as the time consumption for different positioning methods, were analyzed based on real-world datasets. The results show that the standalone UWB positioning system is able to achieve decimeter-level positioning accuracy that is better than 0.3 m in the OXY plane inside the forest canopy even in the presence of severe NLOS propagations. Therefore, this study provides a valuable reference for positioning solutions in robotics-assisted surveying for forestry automation and also in other location-based applications.**

***Index Terms*— Forest canopy, forestry automation, global navigation satellite system (GNSS), positioning, ultrawideband (UWB).**

NOMENCLATURE

d_{true}	True distance.
d_{measured}	Measured distance.
$d_{i,k}$	Measured distance between the tag and the ith beacon at the time step k.
$v_{i,k}$	Distance error between the tag and the ith beacon at the time step k.
δ	Ranging bias.
ω	Random ranging error.
$P_{t,k}$	Location of the tag at time step k.
P_i	Location of the ith beacon.
$\boldsymbol{F}$	Transition matrix.
$\boldsymbol{G}_k$	Backward Kalman gain at the time step k.
$\boldsymbol{H}_k$	Measurement model matrix at the time step k.
$\boldsymbol{x}_k$	State at time step k.
$\boldsymbol{x}_k^s$	Augmented state at time step k.
$\boldsymbol{P}_k$	Covariance of a Kalman filter at the time step k.
$\boldsymbol{P}_k^s$	Augmented covariance at the time step k.
$\boldsymbol{Q}_k$	Covariance of the process noise at the time step k.
$\boldsymbol{R}_k$	Covariance matrix of the measurement at the time step k.
$\boldsymbol{z}_k$	Measurement at time step k.
$\sum$	Sum.
SVD	Singular value decomposition.

Abbreviations

AltDS-TWR	Alternative double-sided two-way ranging.
AGV	Autonomous ground vehicles.
cdf	Cumulative distribution function.
CIR	Channel impulse response.
Ed	Euclidean distance.
EKF	Extended Kalman filter.
ERTSS	Extended Rauch–Tung–Striebel smoother.
FPU	Floating-point unit.
GNSS	Global navigation satellite system.
IMU	Initial measurement unit.
LDE	Leading edge.
LOS	Line-of-sight.
LS	Least squares.
MAX	Maximum error.
NLOS	Non-line-of-sight.
PPS	Pulse per second.
RMSE	Root-mean-square error.
RTK	Real-time kinematics.
RTS	Rauch–Tung–Striebel smoother.
SLAM	Simultaneous localization and mapping.
SS-TWR	Single-side two-way ranging.
STD	Standard deviation.
TDMA	Time-division multiple access.
UAV	Unmanned airborne vehicle.
UWB	Ultrawideband.

Manuscript received 22 December 2023; revised 21 May 2024; accepted 22 May 2024. Date of publication 12 June 2024; date of current version 20 June 2024. This work was supported in part by the Academy of Finland through the UNITE Flagship under Grant 337656, under projects Capturing Structural and Functional Diversity of Trees and Tree Communities for Supporting Sustainable Use of Forests / Consortium: Diversity4Forests under Grant 338644 and Feasibility of Inside-Canopy UAV Laser Scanning for Automated Tree Quality Surveying / Consortium: Quality4Trees under Grant 334002, and in part by the Ministry of Agriculture and Forestry of Finland and European Union NextGenerationEU through the project IlmoStar under Grant VN/27353/2022. The Associate Editor coordinating the review process was Dr. Guanfeng Du. *(Corresponding author: Zuoya Liu.)*

Zuoya Liu, Harri Kaartinen, Teemu Hakala, Juha Hyyppä, and Antero Kukko are with the Department of Remote Sensing and Photogrammetry, National Land Survey of Finland, Finnish Geospatial Research Institute, 02150 Espoo, Finland (e-mail: zliu@maanmittauslaitos.fi; harri.kaartinen@nls.fi; teemu.hakala@nls.fi; juha.coelasr@gmail.com; antero.kukko@nls.fi).

Ruizhi Chen is with the State Key Laboratory of Information Engineering in Surveying, Mapping and Remote Sensing, Wuhan University, Wuhan, Hubei 430072, China (e-mail: ruizhi.chen@whu.edu.cn).

Digital Object Identifier 10.1109/TIM.2024.3413139

© 2024 The Authors. This work is licensed under a Creative Commons Attribution 4.0 License.
For more information, see https://creativecommons.org/licenses/by/4.0/

I. Introduction

FORESTS are of great importance to people in Finland and around the world. Therefore, a larger number of measures and tools have been developed and introduced to gain more knowledge about the forests and to support forest-based green growth and corona crisis recovery in the regions. These outcomes provide timely information for environmental sustainability, economic possibilities, and various ecosystem services, thus helping to balance among all possibilities of multifunctional forestry ranging from economic aspects (timber, pulp, and energy wood) to climate regulation, biodiversity, wildlife, wild berries, and so on.

Currently, surveying and robotic technologies are converging [1], resulting in rapid increase in the demands for robotic-assisted surveying for forest detection, monitoring, and management in recent years due to labor shortages and high labor costs as well as the growing demands for forestry automation applications [2], [3], [4], such as collecting inventory and harvesting. To achieve these targets, a precise and reliable 2-D/3-D positioning solution is needed, especially for these applications in which the robot needs to operate autonomously under canopies with reduced human efforts. In addition, it is also sufficient for multiple robot joints and safe operation under a larger forest canopy simultaneously.

GNSSs are widely used for positioning and navigation outdoors [5], which is an indispensable tool for critical infrastructure tasks such as positioning and navigation for pedestrians and vehicles [6]. However, although GNSS can provide centimeter-level positioning accuracy in outdoor open spaces with RTK techniques [7], [8], the resolution can quickly increase to several tens of centimeters and even to meters if the satellite visibility is obstructed by an overhead canopy [9]. To overcome the environmental limitation of the GNSS measurements, different positioning methods with other types of sensors/measurements have been introduced to enhance the positioning accuracy of GNSS and ensure the consistency and continuity of location information inside forest canopy, such as standalone or fusion UWB positioning [10], [11] and SLAM navigation with/without high-definition map matching using LiDAR/camera data [1], [12], [13], [14].

Liang et al. [15] developed a fully automated undercanopy UAV by using an onboard LiDAR sensor, an IMU sensor, and a camera and demonstrated the feasibility of applying autonomous undercanopy UAV to navigate itself inside a forest canopy and to collect data for forest and tree attribute estimations. Nguyen et al. [16] achieved an uncertainty-aware visually attentive navigation for UAV by only using a depth camera, which can navigate a UAV inside a dense forest autonomously at a flight speed of 2.5 m/s. Ruetz et al. [17] achieved autonomous navigation for AGVs in challenging dense and cluttered vegetated environments by only using a LiDAR sensor. However, although SLAM-based methods have many advantages, such as high accuracy and real-time performance, they usually require a powerful and large-capacity battery for the computing platform and LiDAR/camera as well as other sensors integrated into the system. In addition, the positioning accuracy of the SLAM highly depends on the performance of the LiDAR/camera sensor used. In contrast, UWB-based methods can be easily implemented on a low-power embedded platform, such as an STM32F4 processor; thus, they can achieve an extremely lower energy consumption of less than approximately 1 W [18], which is sufficient for robotic-assisted surveying in the long term. Moreover, the centimeter-level ranging accuracy of UWB technology [19] gives it the possibility to achieve decimeter-level or even centimeter-level positioning accuracy inside forest canopy.

Compared with other radio frequency technologies, such as Bluetooth [20] and Wi-Fi [21] used for close-range communication and positioning as well as 5 G [22] used for long-range communication and close-range positioning, the advantage of UWB technology is its capability to use minimal energy for medium- and long-range communications and distance measurements while maintaining precise timing and anti-interference capabilities [23]. UWB transmits information by generating radio energy at specific time intervals and occupying a large bandwidth instead of varying the power level, frequency, and/or phase of a sinusoidal wave, thus enabling pulse position or time modulation [23]. As a result, the UWB pulse can be used to determine the distance between two devices by measuring the time delay of the pulse traveling between them, thus achieving precise real-time positioning. Moreover, the UWB pulse can travel through walls and other objects, allowing it to reasonably operate and have strong potential in NLOS scenarios [10], such as GNSS-denied forests full of trees.

Currently, UWB positioning is commonly used in indoor environments to locate pedestrians and robotics [24], [25], [26], where LOS propagation can be easily satisfied. However, for GNSS-denied forest environments, very few studies have been performed, especially considering real-world datasets, leading to unexpected challenges in realizing practical applications. Anderson et al. [11] described the propagation characterization of low-antenna UWB signals in four different forest environments with different densities, verifying that UWB propagation in these areas depends heavily on the forest density and antenna type as well as the forest configuration. The frequency range of the UWB pulse used in that study was from 830 to 4200 MHz, which is greater than that of the current state-of-the-art UWB pulse (with a frequency range of 500 MHz); thus, very little is known about the exact performance of the current state-of-the-art UWB signals in forest environments. In addition, Kai et al. [10] presented a valuable UWB positioning study in 2015 in a GNSS-compromised outdoor environment located in the Wayne National Forest near Athens, Ohio, with a set of UWB devices, PulseON 410 ranging and communications module. Similarly, these results are outdated compared to the current state-of-the-art UWB positioning.

Therefore, to determine the exact performance of the current state-of-the-art UWB positioning inside forest canopy, a detailed performance analysis of standalone UWB positioning was performed in this article by using one of the most commonly used UWB chips, DW1000 chip from Decawave, in the market recently in an actual forest environment (see Fig. 1). In addition, four commonly used positioning methods working tightly with/without the smoothing filter were also performed and compared to fully characterize the positioning performance of the system: 1) the linear iterative positioning algorithm, LS and LS-RTS, and 2) the nonlinear recursive positioning algorithm, the EKF and EKF-ERTSS. These four positioning methods can be easily implemented in real time using an embedded processor platform with limited computing ability, such as an STM32F4 processor. Furthermore, a performance comparison for the four positioning

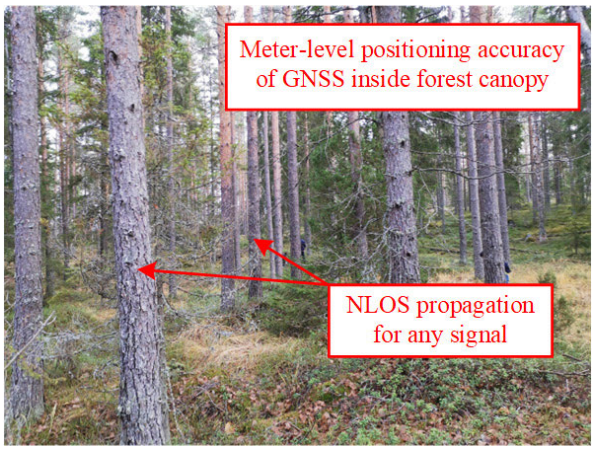

Fig. 1. Live review of the forest environment used for the study.

methods is conducted upon the final outcomes of each method. We also analyzed the minimum update rate of the UWB measurements needed for each method to ensure the positioning performance of the system. The presented experimental results fully demonstrate that standalone UWB positioning is sufficient to bring the meter-level positioning accuracy of GNSS to the decimeter level, less than 0.3 m, in forest environments even with severe NLOS propagation.

The main contributions of this article are highlighted as follows.

1) We perform a detailed performance analysis of standalone UWB positioning inside forest canopy with slight/severe NLOS propagations by using one of the most popular UWB chips in the market, thus providing a valuable reference for the implementation of standalone UWB positioning in forestry automation and other location-based services.
2) To the best of our knowledge, we are the first to characterize the exact performance estimation of 2-D and 3-D for standalone UWB positioning with different positioning update rates in NLOS conditions based on real-world datasets.
3) We discuss the multiuser scalability of standalone UWB positioning inside the forest canopy and provide an optimal solution to serve this application.

The remainder of this article is organized as follows. Section II reviews the methods used for the UWB ranging bias calibration. Section III describes the four estimated positioning methods in detail. Section IV shows the setup of the field tests. Section V presents the experimental results and analysis. Section VI discusses the multiuser scalability and provides an optimal solution. Finally, Section VII offers conclusions.

II. UWB Ranging Bias Calibration

Based on the report of Decawave [19] and the experimental results provided by [27], in addition to the antenna delay, clock drift, and frequency drift, UWB ranging errors are mainly attributed to the variational ranging bias caused by different received signal powers within the distance range. These biases are caused by the inaccurate *Rx* timestamps estimated by the LDE algorithm [28] integrated into the UWB chips and used to find the "LDE" of the CIR of the received signals. The effect has been described and verified in [19]. As a result, the

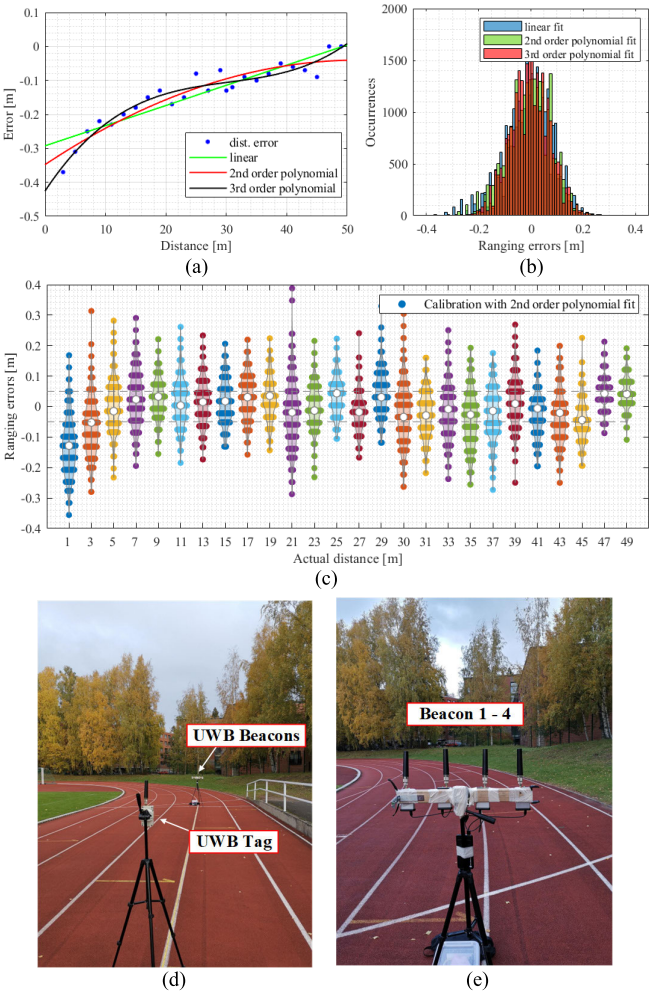

Fig. 2. UWB ranging bias calibration. (a) Calibration with different models. (b) Example of the ranging errors in LOS conditions after the bias calibration. (c) Ranging errors of the calibrated measurements for different distances utilizing the 2nd-order polynomial fit. (d) Tag and beacons. (e) Beacons.

measured distance can be modeled as

$$d_{\text{measured}} = d_{\text{true}} - f(\delta, d_{\text{true}}) - \omega \tag{1}$$

where d_{true} is the true distance, d_{measured} is the measured distance between two UWB devices, δ is the corresponding ranging bias with respect to d_{true}, $f(,)$ is the function between δ and d_{true}, and ω is the random error of the ranging algorithm integrated into the UWB chip. According to [19], a bias that varies with the received signal power level can be observed in the reported timestamp of the received UWB signal, introducing a ranging bias in the evaluated distance measurement. Besides, different ranging biases are included for different true distances. However, based on our previous study [29], it is possible to fit the function between δ and d_{true} in advance with a simple linear function. Thus, the bias with respect to the true distance can be eliminated effectively. Although different functions may appear for different environments, the values of the function variables will change slightly for the same pair of UWB devices under LOS conditions. Therefore, the estimation for the function only needs to be performed once.

Fig. 2(a)–(c) shows an example of the fit results of the bias calibration and an example of the statistic results of the calibrated measurements, and Fig. 2(d) and (e) shows

the test environment used for calibration. The results show that better performance was achieved by the polynomial-based model with an average ranging precision of less than approximately ±7 cm for all the tested distance ranges from 3 to 49 m. Meanwhile, the polynomial-based model outperforms the linear-based model, especially when the close distance was less than 5 m. In addition, as can be seen from Fig. 2(a) and (b), the performance of the 3rd-order polynomial fit is only slightly better than that of the second fit. Therefore, to ensure the ranging precision while keeping the time consumption of the ranging correction unchanged, all the distance measurements in Section IV were collected based on the second polynomial-based model.

Furthermore, different ranging biases are included in the results for different UWB beacons even with respect to the same UWB receiver due to the differences in the components soldered between the UWB chip and antenna [10], [30]. For the UWB modules produced by the same factory at the same time, this effect can be minimized. However, for this study, we used four self-developed UWB devices to perform all the field tests based on DW1000. Therefore, to achieve more accurate UWB positioning, strict calibration is necessary for each pair of UWB beacons and receivers. Toward this goal, the real-world datasets of the ranging measurements without bias calibration were obtained in LOS conditions in an outdoor environment where no multipath propagations were included in this scenario. The distance range was set to 3–49 m with a distance interval of 2 m. A total of 1000 distance measurements were obtained for each distance in the same conditions (weather, temperature, humidity, time of the day, and environment), as shown in Fig. 2(d) and (e). The median of these measurements was used as the final distance measurement. The use of the median instead of the mean is sufficient to eliminate the effect of the ranging outliers on the results, especially in the cases with a small number of measurements. Then, the function between the ranging biases and the true distances can be fit with a linear or polynomial model [10].

In addition, all the errors in Fig. 2(a) are negative. This is because there is an inaccurate antenna delay (an excessively large value) with the UWB device. Normally, it is difficult to measure the true value of the antenna delay for each UWB device because of the difference in the ranging biases caused by the variational received signal level at different distances [29]. However, these biases can be mitigated effectively by fitting the function between δ and d_{true}, as shown in Fig. 2(c).

III. Positioning Methods

For a demonstration of the standalone UWB positioning system, three or four beacons with known locations are necessary to determine the unknown 2-D/3-D locations of the tag, as shown in Fig. 3. Theoretically, the unknown locations of the tag can be determined by calculating the intersection of the three circles in 2-D or at least four spheres in 3-D. However, these circles or spheres rarely intersect at a single location in practice due to inaccurate distance measurements caused by factors such as unfixed ranging bias and NLOS measurements. Fig. 3 demonstrates the possible location area for the tag, the red ellipse with the dotted line.

As mentioned above, we compare and analyze four commonly used positioning methods, LS, LS-RTS, EKF, and EKF-ERTSS, considering that all four methods can be easily implemented in real time using an embedded platform with limited computing ability. Although the particle filter has the best performance for standalone UWB positioning (especially when the target speed is increased) based on the analysis results of [31], the complex calculation of this method heavily limits its real-time applications, especially for an embedded processor platform. Therefore, this article compares and analyzes these four positioning methods. The following contents of this section review the implementation of the four positioning methods in detail one by one.

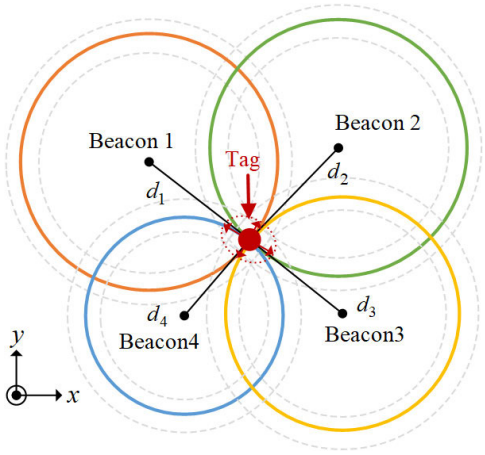

Fig. 3. Illustration of the possible location estimation for the tag in the standalone UWB positioning.

A. Least Squares

Let $P_{t,k} = [x_{t,k}, y_{t,k}, z_{t,k}]^T$ be the location of the tag at estimation time k, and let $P_i = [x_i, y_i, z_i]^T$ be the location of the ith beacon. Then, the basic equation is modeled as

$$v_{i,k} = \left(x_{t,k} - x_i\right)^2 + \left(y_{t,k} - y_i\right)^2 + \left(z_{t,k} - z_i\right)^2 - d_{i,k}^2 \quad (2)$$

where $d_{i,k}$ is the measured distance between the tag and the ith beacon and $v_{i,k}$ is the distance error. Using several distance measurements obtained by the tag at almost the same location for different beacons and supposing that the distance error follows a normal distribution, the optimal solution of the location for the tag can be obtained by LS by minimizing the sum of squared residuals as follows:

$$\min_{x,y,z} \sum_{i,j,k} v_{i,j,k}^2 \left(x_i, y_i, z_i, d_{i,j,k}\right). \quad (3)$$

For (3), a minimum of the three/four distance measurements must be available to determine the optimal location of the tag in 2-D/3-D.

B. Extended Kalman Filter

Usually, precision estimations can be obtained by LS for a static tag due to the fixed network geometry between the static tag and all the stationary beacons. However, for kinematic conditions, inaccurate results may occur due to the continuously changing network geometry and the distance outliers caused by NLOS propagations. To overcome the effects of these factors on positioning and thus improve the robustness of positioning, the EKF is highly available to limit these outliers because the EKF is able to determine to what degree to rely on the measurement or use the predicted estimation to estimate the optimal location for the kinematic conditions.

In the EKF, the state vector stays the same as the standard Kalman filter. Moreover, for standalone UWB positioning with n beacons, the observation vector of the EKF for the measurement update is modeled as

$$z_k = \left[d_{1,k} d_{2,k} \cdots \; d_{n,k}\right]^T \tag{4}$$

where $d_{i,k}$ is the measured distance between the tag and the ith beacon at the estimation time k.

Without considering the velocity and acceleration of the tag, the Jacobian matrix $\boldsymbol{H}_k$ in the EKF is obtained by

$$\boldsymbol{H}_k = \begin{bmatrix} \frac{x_k - x_1}{f_1(k, P_1)} & \frac{y_k - y_1}{f_1(k, P_1)} & \frac{z_k - z_1}{f_1(k, P_1)} \\ \cdots & \cdots & \cdots \\ \frac{x_k - x_n}{f_n(k, P_n)} & \frac{y_k - y_n}{f_n(k, P_n)} & \frac{z_k - z_n}{f_n(k, P_n)} \end{bmatrix} \tag{5}$$

where $f_i(k, P_i) = ((x_k - x_i)^2 + (y_k - y_i)^2 + (z_k - z_i)^2)^{1/2}$.

In addition, the error covariance matrix $\boldsymbol{R}_k$ for the measurement function in the EKF is obtained by

$$\boldsymbol{R}_k = \text{diag}\left[\sigma_{1,k}^2 \sigma_{2,k}^2 \cdots \sigma_{n,k}^2\right]. \tag{6}$$

Then, the location of the tag at estimation time k is using the EKF calculation process.

C. Rauch–Tung–Striebel Smoother and Extend Rauch–Tung–Striebel Smoother

The RTS, also called Kalman smoother, can be implemented to smooth the locations obtained by the LS-based method [32], [33], thus restraining the bounce points obtained in the trajectory. Similarly, its special case, ERTSS, can be implemented to smooth the locations obtained by the EKF-based method by replacing the prediction equations with first-order approximations. Toward this goal, the constant velocity kinematic model is commonly used as the motion model for the kinematic tag in both RTS and ERTSS. Based on this, the corresponding parameters at the estimation time k in both RTS and ERTSS are defined as

$$\boldsymbol{x}_k = \left[xyz\right]^T, \boldsymbol{P}_k = \text{diag}\left[\delta_{x,k}^2 \delta_{y,k}^2 \delta_{z,k}^2\right] \tag{7a}$$

$$\boldsymbol{Q}_k = \text{diag}\left[T^4/4 T^4/4 T^4/4\right] \cdot \delta_{w,k}^2 \tag{7b}$$

where x, y, and z are the coordinates of the state, T is the time interval of the measurement updates, $\boldsymbol{P}_k$ is the covariance estimate of the filter, and $\boldsymbol{Q}_k$ is the covariance of the process noise. In practical positioning applications, T should be set as small as possible so that the velocity over this interval is assumed to be nearly constant. The smoothing state estimation and the covariance matrix in the RTS are obtained by

$$\boldsymbol{x}_{k+1}^- = \boldsymbol{F}_k \boldsymbol{x}_k \tag{8a}$$

$$\boldsymbol{P}_{k+1}^- = \boldsymbol{F}_k \boldsymbol{P}_k \boldsymbol{F}_k^T + \boldsymbol{Q}_k \tag{8b}$$

$$\boldsymbol{G}_k = \boldsymbol{P}_k \boldsymbol{F}_k^T \left(\boldsymbol{F}_k \boldsymbol{P}_k \boldsymbol{F}_k^T + \boldsymbol{Q}_k\right)^{-1} \tag{8c}$$

$$\boldsymbol{x}_k^s = \boldsymbol{x}_k + \boldsymbol{G}_k \left(\boldsymbol{x}_{k+1}^s - \boldsymbol{x}_{k+1}^-\right) \tag{8d}$$

$$\boldsymbol{P}_k^s = \boldsymbol{P}_k + \boldsymbol{G}_k \left(\boldsymbol{P}_{k+1}^s - \boldsymbol{P}_{k+1}^-\right) \boldsymbol{G}_k^T \tag{8e}$$

where $\boldsymbol{F}_k = \text{diag}[1\ 1\ 1]$ is the transition matrix of the jump from the time step k to time step $k+1$, $\boldsymbol{G}_k$ is the backward Kalman gain, and $\boldsymbol{x}_k^s$ and $\boldsymbol{P}_k^s$ are the augmented state and covariance estimate, respectively. Based on [29], the original derivation of the Kalman filter (linear filter) was based on the LS approach. Thus, we can use RTS to smooth the results obtained by the LS. For LS-RTS, $\boldsymbol{Q}_k$ and $\boldsymbol{P}_k$ were set as fixed values as follows: $\boldsymbol{Q}_k = \boldsymbol{P}_k = \text{diag}[0.0150.0150.0001]$.

Different from the RTS, the transition matrices of 9(b) and 9(c) in the ERTSS are replaced by the evaluated Jacobian matrix in the EKF. Therefore, the smoothing state estimation and covariance matrix in the ERTSS are obtained by

$$\boldsymbol{x}_{k+1}^- = \boldsymbol{F}_k \boldsymbol{x}_k \tag{9a}$$

$$\boldsymbol{P}_{k+1}^- = \boldsymbol{H}_k \boldsymbol{P}_k \boldsymbol{H}_k^T + \boldsymbol{Q}_k^- \tag{9b}$$

$$\boldsymbol{G}_k = \boldsymbol{P}_k \boldsymbol{H}_k^T \left(\boldsymbol{H}_k \boldsymbol{P}_k \boldsymbol{H}_k^T + \boldsymbol{Q}_k^-\right)^{-1} \tag{9c}$$

$$\boldsymbol{x}_k^s = \boldsymbol{x}_k + \boldsymbol{G}_k \left(\boldsymbol{x}_{k+1}^s - \boldsymbol{x}_{k+1}^-\right) \tag{9d}$$

$$\boldsymbol{P}_k^s = \boldsymbol{P}_k + \boldsymbol{G}_k \left(\boldsymbol{P}_{k+1}^s - \boldsymbol{P}_{k+1}^-\right) \boldsymbol{G}_k^T \tag{9e}$$

where $\boldsymbol{Q}_k^-$ is the covariance of the process noise with $\delta_{w,k} = \text{sum}(\text{SVD}(\boldsymbol{P}_{k-1}))T_k$, $T_k = t_k - t_{k-1}$ is the time interval of the EKF prediction and update, and SVD is the singular value decomposition.

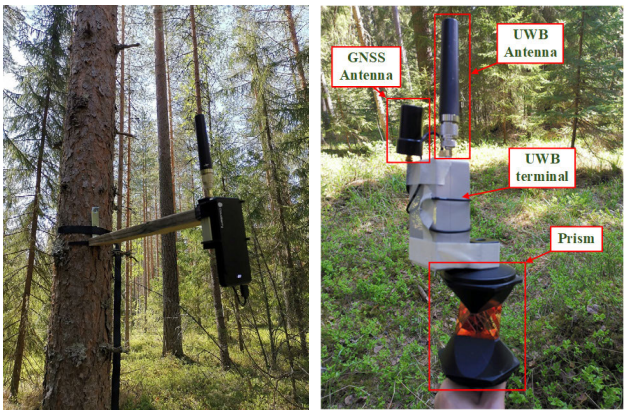

Fig. 4. UWB devices used for the study, UWB beacon (*left*) and UWB receiver (*right*). The size of the field test was larger than 3000 m^2.

IV. Experiment Setup

To characterize the performance of standalone UWB positioning inside forest canopy and to compare and analyze different positioning methods mentioned within the positioning section, a typical forest environment was tested in managed boreal forest sites located in Evo, southern Finland (61°11'28″N, 25°07'00″E). This forest is full of pines with diameters of approximately 20–35 cm, as shown in Figs. 1 and 4.

Fig. 4 shows the bespoke UWB devices used for this study. These UWB beacons were deployed on the trees with a specific bracket with a length of approximately of 0.5 m to keep the UWB beacon as far away from the tree stem as possible and powered by a power bank, and the true locations of all the UWB beacons with respect to each other in the forest were measured by the total station with centimeter-level accuracy. The UWB receiver was mounted with the tracking prism and held by a tester, who was walking freely in the forest to collect the raw distance measurements for postprocessing and analysis. Moreover, a low-cost WPI4130 GNSS module that integrates a U-BLOX NEO-7 GNSS receiver was also integrated into the receiver to provide a unique timestamp for each distance measurement. Therefore, we can estimate the positioning performance of the system by searching the correct timestamps and comparing the corresponding location

TABLE I
CONFIGURATION OF THE DW1000 CHIP

Parameter	Channel	PRF*	Preamble length	Data rate
value	2	64 MHz	512	110 kbps

* PRF denotes the pulse repetition frequency.

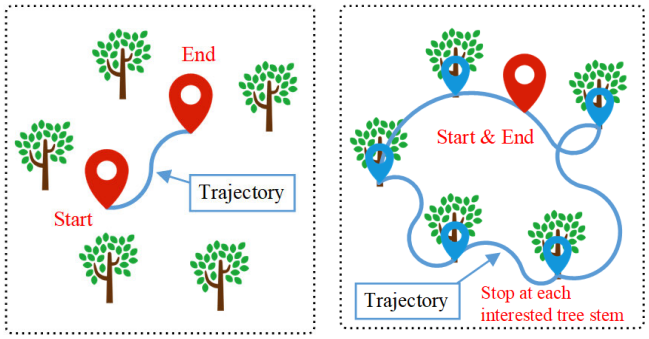

(a) (b)

Fig. 5. Setups for the field tests. For trajectory 2, let the UWB receiver be as close as possible to the tree stem and stay for approximately 3–5 s, and ensure that the tracking prism is always in LOS conditions. (a) Trajectory 1: slight NLOS. (b) Trajectory 2: serious NLOS.

points with respect to the results of the tracking prism, which allows for a comparison of the standalone UWB positioning with high-quality ground truth.

In addition, all the measurements were communicated to a smartphone equipped with the tester via Bluetooth for post-processing and analysis. Moreover, the biases for each pair of UWB receivers and beacons were corrected in advance based on the calibration method within the process flow. However, we only used the polynomial model, and the fit parameters were integrated into the UWB receiver; thus, no postprocessing is necessary for the obtained distance measurements. The ranging algorithm between the UWB receiver and the UWB beacon was SS-TWR, which can achieve ±10-cm ranging accuracy in LOS conditions [34]. The ranging rate was set to 20 Hz per round for all the beacons from number 1 to number 4. The parameters of the DW1000 chip used in this forest are listed in Table I.

Furthermore, two cases were tested, as shown in Fig. 5. The first is when the tester walked along the specific route continuously from the starting point to the endpoint, marked as Trajectory 1. In this case, slight NLOS propagations of UWB signals exist between the kinematic receiver and stationary beacons. The total length of the route is approximately 100 m. The second is when the tester walked randomly in the forest and placed the receiver close to the tree stems, staying for approximately 3–5 s, marked as Trajectory 2. In this case, serious NLOS propagations of UWB signals are involved due to the occlusion of the tree stems because more than 60 trees were involved in this test. This test lasted for approximately half an hour continuously. Overall, these two cases allowed for a full comparison and performance analysis of standalone UWB positioning inside forest canopy with NLOS conditions.

The positioning accuracy of the trajectory is evaluated by calculating the Ed between the estimated location points and the results of the total station by searching the unique timestamps obtained from the GNSS module. First, we searched for the nearest reference points for which less than a 0.01-s time

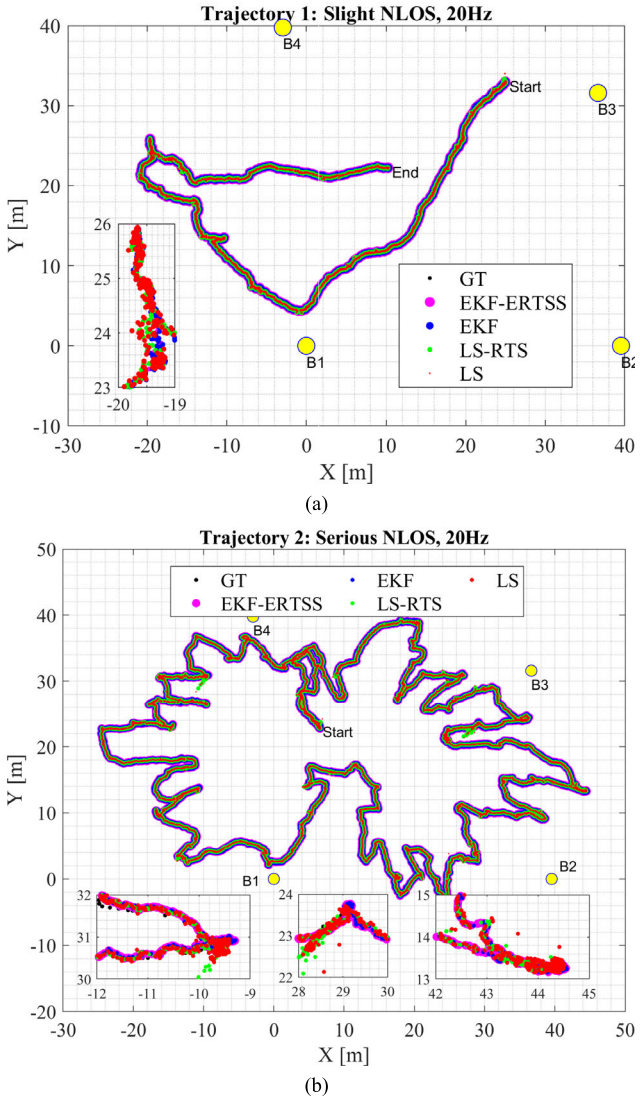

(a)

(b)

Fig. 6. Trajectories of the four positioning methods in the *OXY* plane for the two field tests. (a) Trajectory 1: slight NLOS. (b) Trajectory 2: serious NLOS.

difference was obtained between the location point and the reference point. Then, we calculated the corresponding Ed between them as follows:

$$\text{2DError} = \sqrt{(x_e - x_r)^2 + (y_e - y_r)^2} \tag{10a}$$

$$\text{3DError} = \sqrt{(x_e - x_r)^2 + (y_e - y_r)^2 + (z_e - z_r)^2} \tag{10b}$$

where (x_e, y_e, z_e) denotes the found location point and (x_r, y_r, z_r) is the location of the reference point. Although this approach does not permit the precise determination of the point-to-point positioning error, it can be used to roughly assess the overall positioning accuracy of a solution and compare the performance of different positioning methods.

V. EXPERIMENTAL RESULTS AND PERFORMANCE ANALYSIS

A. Comparison and Performance Analysis for Slight NLOS and Serious NLOS Conditions

Fig. 6 shows the estimated 2-D trajectories in the *OXY* plane for the slight NLOS and serious NLOS conditions

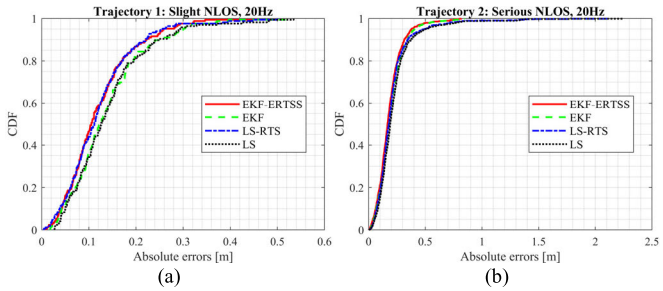

Fig. 7. CDFs of positioning accuracy of the four positioning methods in the *OXY* plane for (a) and (b) Trajectories 1 and 2.

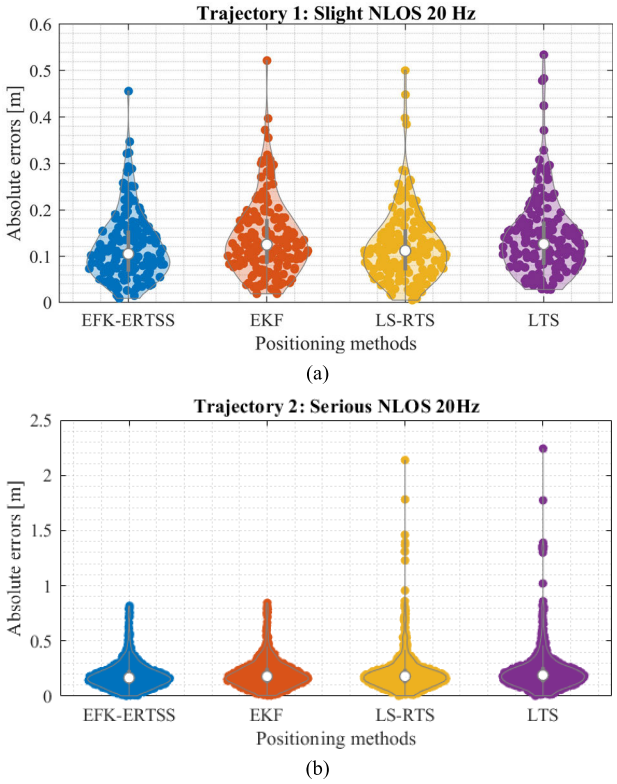

Fig. 8. Positioning errors of the four positioning methods in the *OXY* plane for (a) and (b) Trajectories 1 and 2.

with the four positioning methods mentioned within the positioning section. Figs. 7 and 8 show the corresponding CDFs and boxplots of the errors, respectively. Table II shows the statistical results, including the RMSE, STD, MAX, and 68%–95% errors of the CDFs. The results show that the RMSEs of standalone UWB positioning are less than 0.3 m for both trajectories and all positioning methods. In particular, the RMSEs are less than 0.25 m for both trajectories with the EKF-ERTSS and EKF-based positioning methods. This indicates that standalone UWB positioning is sufficient and capable of bringing the meter-level positioning errors of GNSS inside forest canopy with NLOS conditions to the decimeter level.

As mentioned, the SS-TWR was used as the ranging algorithm between the UWB receiver and beacon, and a ±10-cm ranging accuracy can be achieved by the SS-TWR. As a result, we achieved a positioning accuracy of better than 0.3 m. However, based on the study presented in [34], the AltDS-TWR method is more accurate than SS-TWR, and

TABLE II
STATISTICAL RESULTS OF THE 2-D LOCATION POINTS IN THE *OXY* PLANE, UNIT [m]

Item	Method	RMSE	STD	MAX	68%	95%
Trajectory 1	EKF-ERTSS	**0.14**	0.07	0.45	0.13	**0.26**
	EKF	**0.16**	0.08	0.52	0.15	**0.29**
	LS-RTS	**0.15**	0.08	0.50	0.13	**0.25**
	LS	**0.17**	0.09	0.53	0.15	**0.29**
Trajectory 2	EKF-ERTSS	**0.22**	0.12	0.81	0.20	**0.38**
	EKF	**0.23**	0.12	0.84	0.22	**0.41**
	LS-RTS	**0.28**	0.18	2.14	0.21	**0.51**
	LS	**0.30**	0.19	2.24	0.23	**0.52**

based on the experimental results provided in [25], a ranging accuracy better than ±5 cm can be achieved by AltDS-TWR for the DW1000 chip. Therefore, we can predict that a positioning accuracy better than 0.15 m might be achieved for standalone UWB positioning inside the forest canopy by using the AltDS-TWR method to perform the ranging between the UWB receiver and beacon.

As shown in Fig. 7(a), the performance of the EKF-based method is only slightly better than that of the LS-based method. However, for trajectory 2, under serious NLOS conditions, the EKF-based method achieves better performance, as indicated in Fig. 7(b). In addition, the performance of EKF-ERTSS and LF-RTS is better than that without the smothers. Therefore, we conclude that the EKF-based method is more stable than the LS-based method and that smoother is of great significance to improve the positioning accuracy of the filter.

In addition, the statistical results clearly show that the performance of the EKF-based positioning methods is clearly better than that of the LS-based methods, especially for trajectory 2, serious NLOS conditions. For example, the RMSEs and 95% errors of the EKF-ERTSS-based method are 0.22–0.38 m for trajectory 2, improving by 21%–25% compared to the LS-RTS-based method. Moreover, EKF-based methods achieved a better ability to suppress positioning outliers according to the statistical results of Fig. 8. However, for slight NLOS conditions in which fewer outliers are included in the raw distance measurements, the LS-based methods achieve considerable positioning performance with EKF-based methods. Therefore, for some applications in which LOS conditions can always be served, LS-based methods are also desirable with high-quality positioning performance and reliability. For example, UWB technology can be used to locate a robot in an open environment.

Furthermore, the statistical results also clearly show that the performance with smoothing is slightly better than that without smoothing. Theoretically, smoothing is sufficient to restrain the outliers included in the trajectory, making the estimated trajectory closer to the true trajectory and thus improving the positioning accuracy and enhancing the reliability of the system. However, our update rate of the UWB measurements is set to 20 Hz, which is very fast for a positioning system; thus, the location changes very little during this time interval. As a result, the positioning results can be corrected immediately even without smoothing, but this effect will be weakened for a lower update rate, as demonstrated in the following results

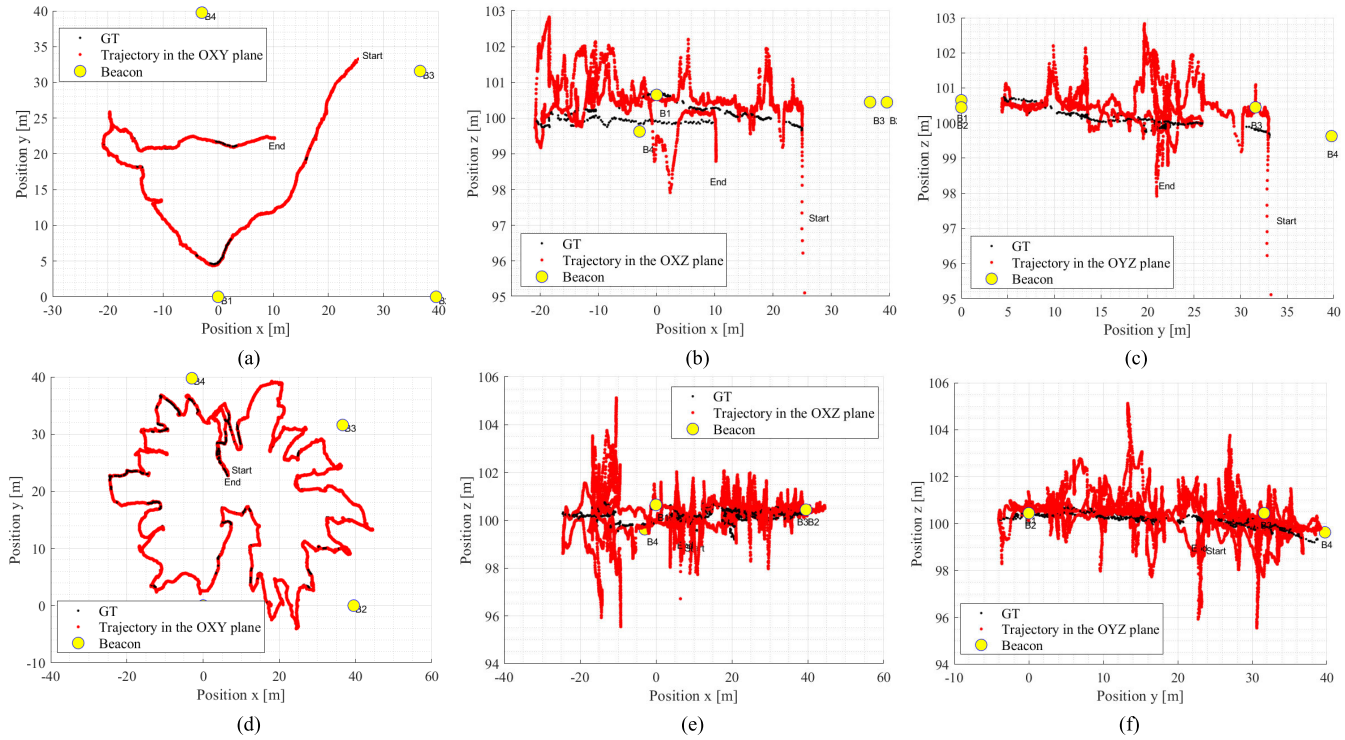

Fig. 9. Results of EKF-ERTSS in the *OXY*, *OXZ*, and *OYZ* planes for Trajectories 1 and 2. (a)–(c) Trajectory 1. (d)–(f) Trajectory 2.

obtained from different update rates. In addition, four ranging measurements were used simultaneously in the positioning methods; thus, accurate location estimations can be obtained even if there are larger ranging errors or outliers included in one or two ranging measurements. For the EKF-based method, this effect can be effectively restrained due to the implementation of the state prediction and measurement update in the method. However, for the LS-based method, the performance may degrade because a good network geometry is the foundation of this method. As shown in Fig. 6, several locations deviated from the ground truth for both LS-RTS- and LS-based methods.

Finally, Fig. 9 shows the 3-D positioning results of the EKF-ERTSS in the *OXY*, *OXZ*, and *OYZ* planes for Trajectories 1 and 2, and Table III shows the corresponding statistical results, including the RMSEs, STDs, MAXs, and 68%–95% errors of the CDFs for the four positioning methods. These results show that the positioning is extremely unreliable when reporting data in the Z-axis, especially for these location points outside the public coverage of the beacons. The maximum positioning errors even increase to 4 m. This is mainly attributed to the impeded network geometry in these areas and the NLOS measurements. Although the positioning accuracies of most location points inside the public coverage on the Z-axis are less than ± 1 m, some outliers are still included in the results. This is mainly caused by inaccuracy in the NLOS measurements. Moreover, the data show that the beacons were almost deployed on the same vertical plane, which is also not sufficient for 3-D positioning even for public coverage.

To obtain accurate 3-D positioning results, better network geometries with more beacons are sufficient to achieve this target. For example, increasing one or two beacons with a height difference larger than 5 m with respect to the four beacons into the network and ensuring that the possible motion routes of the UWB receiver are inside the 3-D coverage of all the beacons. In this way, a good 3-D network geometry for the UWB receiver can be obtained. Furthermore, fusion-based solutions, for example, UWB fusions with IMU sensors, are also sufficient to achieve this target.

B. Comparison and Performance Analysis for Different Positioning Update Rates

To continue characterizing the performance of standalone UWB positioning inside forest canopy and provide valuable references for the actual implementation of the system, in this section, we compared and analyzed the effect of the system positioning update date on the positioning performance. However, we just compared the 2-D positioning results in the *OXY* plane, considering the actual case that the 3-D positioning performance is extremely unstable and inaccurate. The corresponding results are given as follows.

Fig. 10 shows the estimated trajectories, Fig. 11 shows the RMSEs of the four positioning methods with different update rates (1, 2, 5, 10, and 20 Hz) for Trajectories 1 and 2, and Fig. 12 shows the corresponding CDFs. Finally, Tables IV and V show the statistical results for Trajectories 1 and 2, respectively, including the RMESs, STDs, MAXs, and 68% and 95% errors of the CDFs.

It can be seen from Fig. 10 that all positioning update rates achieved good positioning and tracking for the UWB terminal. The results of Tables IV and V show that the standalone UWB positioning system achieved a decimeter-level positioning accuracy better than 0.3 m for both trajectories, even with a 1-Hz positioning update rate for the four positioning methods. Moreover, for Trajectory 1: slight NLOS, the positioning errors are even less than 0.2 m when the positioning update rate is larger than 2 Hz for the four positioning methods.

TABLE III
STATISTICAL RESULTS OF THE 3-D LOCATION POINTS ON THE *X*-, *Y*-, AND *Z*-AXES, UNIT [m]

Item	Method	RMSE			STD			MAX			68%			95%		
		X	Y	Z	X	Y	Z	X	Y	Z	X	Y	Z	X	Y	Z
Trajectory 1	EKF-ERTSS	0.11	0.08	**0.98**	0.11	0.08	**0.71**	0.45	0.29	3.14	0.10	0.07	0.85	0.22	0.17	2.05
	EKF	0.13	0.08	**0.98**	0.13	0.08	**0.72**	0.52	0.29	3.13	0.12	0.08	0.84	0.25	0.18	2.02
	LS-RTS	0.14	0.19	**0.92**	0.14	0.19	**0.80**	0.50	0.85	3.31	0.12	0.15	0.61	0.29	0.42	2.16
	LS	0.16	0.22	**0.98**	0.16	0.21	**0.88**	0.59	1.00	3.30	0.13	0.17	0.70	0.32	0.46	2.07
Trajectory 2	EKF-ERTSS	0.16	0.14	**0.82**	0.15	0.14	**0.82**	0.79	0.76	4.91	0.15	0.12	0.59	0.31	0.28	1.59
	EKF	0.17	0.15	**0.82**	0.16	0.15	**0.82**	0.82	0.77	4.93	0.16	0.14	0.59	0.32	0.31	1.58
	LS-RTS	0.20	0.24	**0.73**	0.19	0.24	**0.72**	0.85	1.54	4.71	0.19	0.18	0.49	0.40	0.48	1.47
	LS	0.21	0.27	**0.79**	0.21	0.27	**0.78**	0.96	1.73	5.10	0.20	0.19	0.54	0.42	0.49	1.70

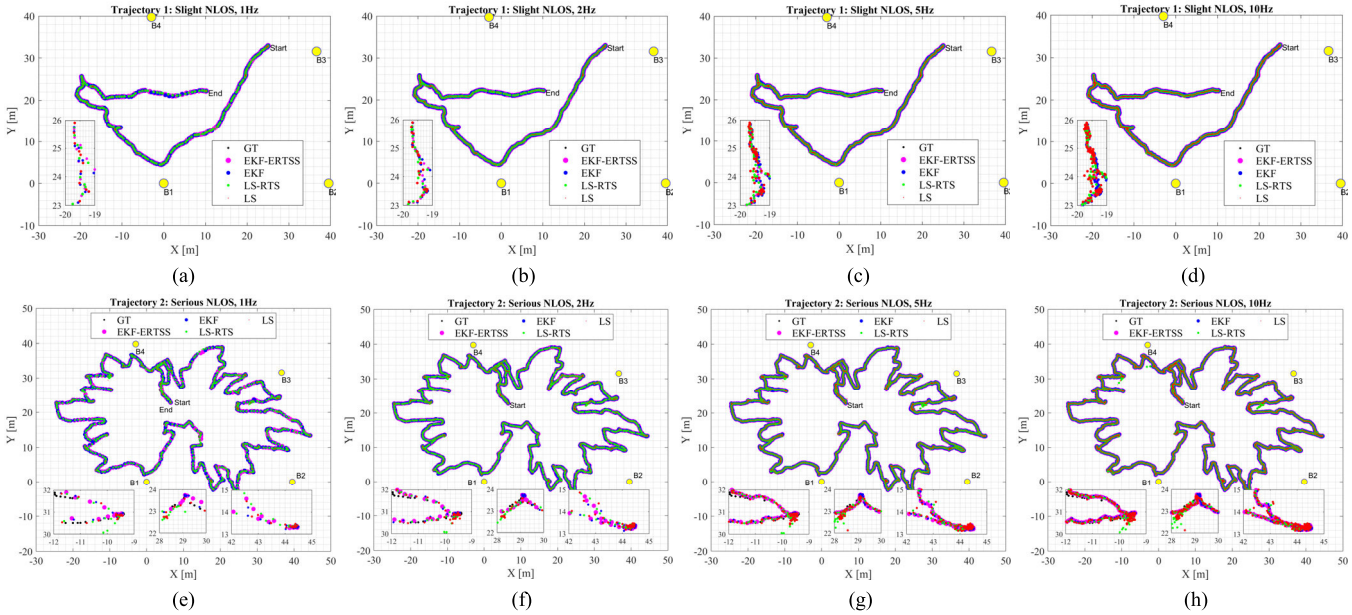

Fig. 10. Positioning results of different update rates for Trajectories 1 and 2. (a)–(d) Trajectory 1. (e)–(h) Trajectory 2.

In addition, Fig. 11 clearly shows that the positioning accuracies increase slightly with the decrease in the update rates from 20 to 5 Hz, marking this case as Case 1. However, the positioning accuracies decrease with the decrease in the update rates from 5 to 2 Hz, especially for EKF-based positioning methods, marking this case as Case 2. For Case 1, this might occur because of the reduced location points that were used to calculate the positioning accuracy, where each location point does not correspond to an actual reference point from the results of the total station due to the occlusion of the tree stem on the tracking prism. For Case 2, the reduced location points are also one of the main sources of error, and another source is that the error model and the motion model are no longer suitable for the positioning methods due to the larger time interval between two continuous location points, especially for the EKF-based methods based on the nonlinear recursive technique. However, for the LS-based methods, a slight difference exists in the positioning results for different update rates, especially for Trajectory 1: slight NLOS. This means that the errors will not accumulate during the motion process for iterative positioning methods. In addition, the timestamp errors of the measurements will also introduce errors in the accuracy estimation.

Furthermore, it is clearly visible from the results of Figs. 11 and 12 that the smoothing performance is only effective for high positioning update rates, for example, 5, 10, and 20 Hz. In addition, it is also clear that the performance of the EKF-based positioning methods is better than that of LS-based methods, especially when the positioning update rates are larger than 5 Hz, which benefits from the implementation of the recursive process in the EKF. However, better performance is obtained by the LS-based method for a 1-Hz positioning update rate due to the invalidation of the recursive process of the EKF.

As shown in Fig. 12 and Tables IV and V, we can also conclude that the EKF-based method is more stable than the LS-based method and that smoother is of great significance to improve the positioning accuracy of the filter, especially when the positioning update rates are larger than 5 Hz. However, in the case of low positioning update dates, such as 2–1 Hz, the performance of smoother is extremely unstable. For example, for trajectory 1 with the positioning update rates of 2 Hz,

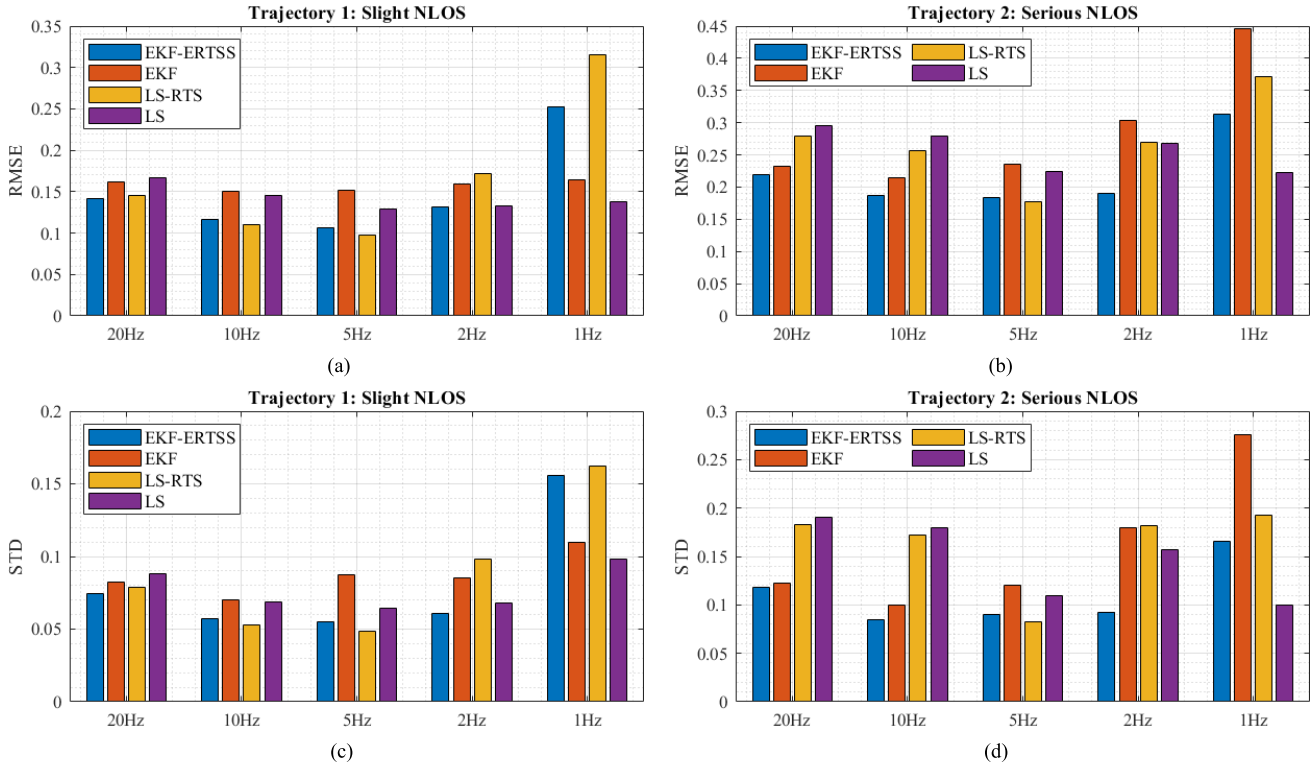

Fig. 11. RMSEs and STDs of different positioning update rates for Trajectories 1 and 2. Note that the accuracy of Fig. 11 is set to 0.01 m to unify the accuracy of these data with the statistical results shown in Tables IV and V. (a) RMSE of Trajectory 1: slight NLOS. (b) RMSE of Trajectory 2: serious NLOS. (c) STD of Trajectory 1: slight NLOS. (d) STD of Trajectory 2: serious NLOS.

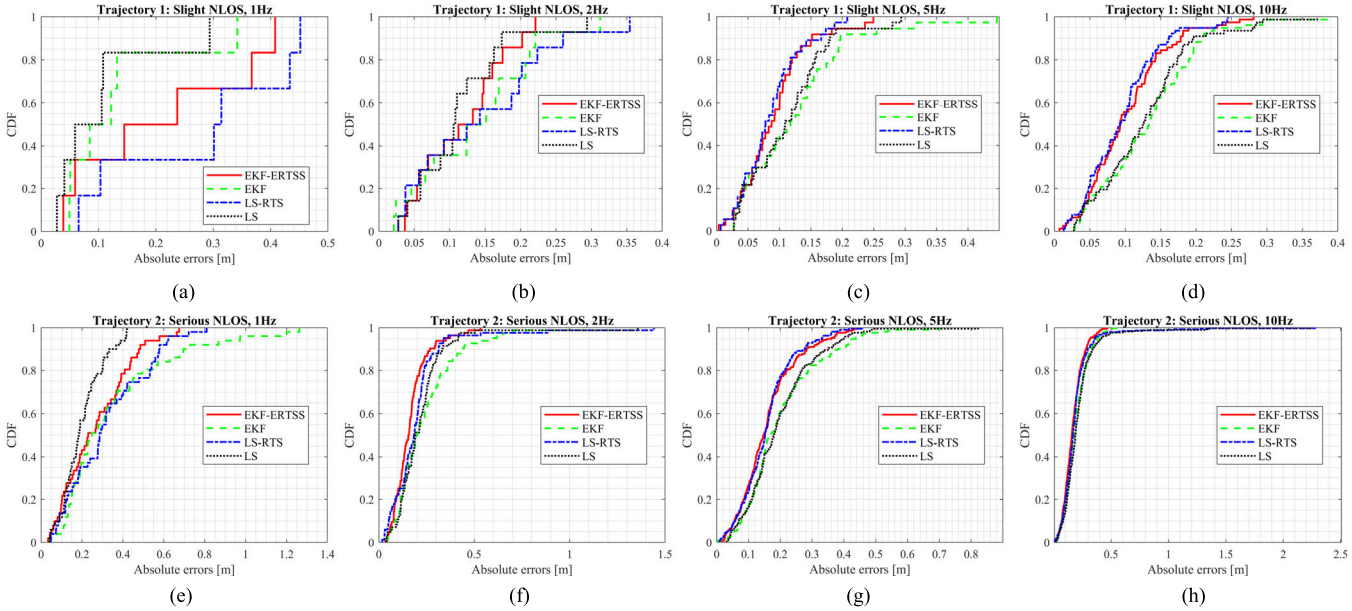

Fig. 12. Corresponding CDFs of different uprate rates for Trajectories 1 and 2. (a)–(d) Trajectory 1. (e)–(h) Trajectory 2.

the performance of LS is much better than that of LS-RTS. The same results can be obtained from Fig. 11. Therefore, we conclude that in order to improve the accuracy of the filter by integrating a corresponding smoother, a positioning update rate of larger than 2 Hz is necessary for both EKF and LS.

In addition, considering the positioning update rate, the performance of the EKF-ERTSS/LS-RTS at 5 Hz is better than that at 20 Hz, as shown in Fig. 11, Tables IV and V. To further analyze this phenomenon, Fig. 13 shows the RMSEs of different starting points used to estimate the performance of the EKF-ERTSS at 5 Hz from the original target of 20 Hz. It is clearly visible that the performance highly depends on the selected index used to determine the results. For example, the performance of $I = 1$ is better than that of $I = 2$ or $I = 4$. Besides, the performance at 5 Hz is mostly better than that at 20 Hz. However, the performance of $I = 4$

TABLE IV
STATISTICAL RESULTS OF THE 2-D LOCATION POINTS IN THE *OXY* PLANE FOR TRAJECTORY 1, UNIT [m]

Item	Method	20 Hz			10 Hz			5 Hz			2 Hz			1 Hz		
		X	Y	XY	X	Y	XY	X	Y	XY	X	Y	XY	X	Y	XY
RMSE	EKF-ERTSS	0.12	0.08	**0.14**	0.09	0.08	**0.12**	0.07	0.08	**0.11**	0.10	0.09	**0.13**	0.18	0.18	**0.25**
	EKF	0.14	0.09	**0.16**	0.12	0.09	**0.15**	0.12	0.09	**0.15**	0.13	0.10	**0.16**	0.16	0.05	**0.16**
	LS-RTS	0.12	0.08	**0.15**	0.08	0.07	**0.11**	0.07	0.06	**0.10**	0.13	0.11	**0.17**	0.24	0.21	**0.32**
	LS	0.14	0.10	**0.17**	0.11	0.09	**0.15**	0.11	0.07	**0.13**	0.10	0.08	**0.13**	0.12	0.07	**0.14**
STD	EKF-ERTSS	0.12	0.08	**0.07**	0.09	0.08	**0.06**	0.07	0.08	**0.05**	0.10	0.09	**0.06**	0.18	0.16	**0.16**
	EKF	0.14	0.09	**0.08**	0.12	0.09	**0.07**	0.12	0.09	**0.09**	0.13	0.10	**0.09**	0.15	0.05	**0.11**
	LS-RTS	0.12	0.08	**0.08**	0.08	0.07	**0.05**	0.06	0.07	**0.05**	0.13	0.11	**0.10**	0.24	0.19	**0.16**
	LS	0.14	0.10	**0.09**	0.11	0.09	**0.07**	0.09	0.08	**0.06**	0.10	0.09	**0.07**	0.11	0.07	**0.10**
MAX	EKF-ERTSS	0.45	0.27	**0.45**	0.27	0.19	**0.28**	0.23	0.15	**0.25**	0.22	0.16	**0.22**	0.30	0.37	**0.41**
	EKF	0.52	0.25	**0.52**	0.38	0.19	**0.39**	0.39	0.22	**0.45**	0.30	0.21	**0.31**	0.34	0.07	**0.34**
	LS-RTS	0.47	0.44	**0.50**	0.25	0.23	**0.25**	0.20	0.16	**0.21**	0.35	0.25	**0.35**	0.37	0.40	**0.45**
	LS	0.48	0.52	**0.53**	0.37	0.29	**0.37**	0.28	0.20	**0.29**	0.28	0.16	**0.29**	0.28	0.10	**0.29**
68%	EKF-ERTSS	0.11	0.07	**0.13**	0.08	0.08	**0.12**	0.06	0.08	**0.11**						
	EKF	0.12	0.19	**0.15**	0.12	0.10	**0.16**	0.13	0.18	**0.15**						
	LS-RTS	0.11	0.07	**0.13**	0.08	0.07	**0.11**	0.06	0.06	**0.10**		#			#	
	LS	0.13	0.09	**0.15**	0.13	0.09	**0.15**	0.12	0.07	**0.14**						
95%	EKF-ERTSS	0.24	0.15	**0.26**	0.18	0.16	**0.23**	0.20	0.15	**0.19**						
	EKF	0.28	0.18	**0.29**	0.20	0.18	**0.26**	0.30	0.19	**0.32**		#			#	
	LS-RTS	0.23	0.16	**0.25**	0.14	0.15	**0.23**	0.17	0.16	**0.19**						
	LS	0.27	0.18	**0.29**	0.19	0.19	**0.28**	0.19	0.18	**0.28**						
Number of the location points		166			74			37			14			6		

# denotes the results are not meaningful because the number of the location points is too small to estimate the positioning accuracy.

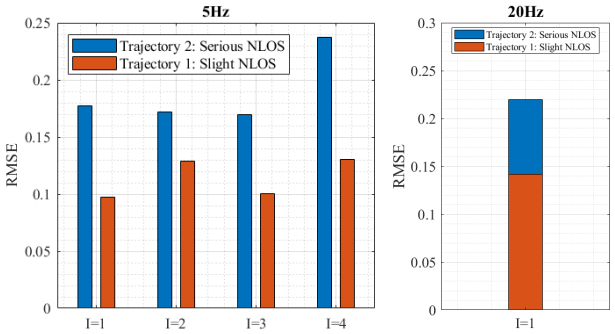

(a) (b)

Fig. 13. (a) RMSEs of different starting points used to estimate the performance of the EKF-ERTSS at 5 Hz from the original target for Trajectories 1 and 2. (b) RMSEs of the original target of 20 Hz. I denotes the index of the starting point. All the results were obtained based on the EKF-ERTSS method.

at 5 Hz is comparable to that at 20 Hz. This is mainly caused by the method used to determine the positioning accuracy. As mentioned before, we first searched for the nearest reference points for which less than a 0.01-s time difference was obtained between the location point and the reference point. Then, we calculated the corresponding Ed between them based on (10). Therefore, for the results at 20–5 Hz, different estimated locations will be used to calculate the accuracy. Besides, more location points will also be used to estimate the results at 20 Hz. However, most searched location points of $I = 4$ at 5 Hz remain basically the same as those at 20 Hz. Thus, the performance in the two cases is comparable to each other.

Finally, Table VI shows the comparison of the time consumption for the four positioning methods. All the estimations were obtained with postprocessing, and the configuration of the PC is given as follows: 1) processor, 11th Gen Inter[1] Core[2] i7-11 800 H @ 2.30 GHz, and 2) RAM, 64 GB. From these results, it can be seen that the time consumption of the EKF-based methods increases by approximately 50% compared with LS-based methods. Therefore, for real-time positioning applications with an embedded processor, such as STM32F4, LS-based methods might be more sufficient. For the LS, a fixed number of calculations are enough to obtain the results precisely. For example, calculations were performed ten times in this study. For the EKF, it is better to use an embedded processor integrated with an FPU to perform the positioning in real time because it can perform complexity matrix computation in real time without losing the precision. However, this also depends on the degree of the optimization for the positioning algorithm and thus needs to be estimated in the real world. This is not the focus of this article. For some applications, using a lower positioning update

[1]Registered trademark.
[2]Trademarked.

TABLE V
STATISTICAL RESULTS OF THE 2-D LOCATION POINTS IN THE *OXY* PLANE FOR TRAJECTORY 2, UNIT [m]

Item	Method	20 Hz			10 Hz			5 Hz			2 Hz			1 Hz		
		X	Y	XY	X	Y	XY	X	Y	XY	X	Y	XY	X	Y	XY
RMSE	EKF-ERTSS	0.17	0.14	**0.22**	0.14	0.12	**0.19**	0.14	0.12	**0.18**	0.14	0.13	**0.19**	0.23	0.22	**0.31**
	EKF	0.18	0.15	**0.23**	0.16	0.14	**0.21**	0.17	0.17	**0.24**	0.20	0.23	**0.30**	0.23	0.38	**0.45**
	LS-RTS	0.20	0.19	**0.28**	0.18	0.18	**0.26**	0.14	0.11	**0.18**	0.20	0.18	**0.27**	0.29	0.23	**0.37**
	LS	0.21	0.21	**0.30**	0.20	0.20	**0.28**	0.17	0.15	**0.22**	0.19	0.19	**0.27**	0.16	0.15	**0.22**
STD	EKF-ERTSS	0.16	0.14	**0.12**	0.13	0.12	**0.08**	0.13	0.12	**0.09**	0.13	0.13	**0.09**	0.23	0.21	**0.17**
	EKF	0.17	0.15	**0.12**	0.15	0.14	**0.10**	0.15	0.17	**0.12**	0.19	0.23	**0.18**	0.22	0.38	**0.28**
	LS-RTS	0.19	0.19	**0.18**	0.17	0.18	**0.17**	0.13	0.11	**0.08**	0.19	0.18	**0.18**	0.29	0.24	**0.19**
	LS	0.21	0.21	**0.19**	0.19	0.20	**0.18**	0.15	0.15	**0.11**	0.19	0.19	**0.16**	0.15	0.15	**0.10**
MAX	EKF-ERTSS	0.79	0.79	**0.81**	0.39	0.46	**0.47**	0.40	0.43	**0.44**	0.42	0.52	**0.53**	0.66	0.67	**0.67**
	EKF	0.81	0.80	**0.84**	0.47	0.47	**0.55**	0.47	0.60	**0.72**	0.62	1.16	**1.23**	0.70	1.25	**1.26**
	LS-RTS	1.38	1.63	**2.14**	1.46	1.75	**2.28**	0.41	0.45	**0.46**	0.93	1.10	**1.44**	0.80	0.57	**0.81**
	LS	1.44	1.72	**2.24**	1.44	1.72	**2.24**	0.47	0.80	**0.82**	0.89	1.02	**1.36**	0.34	0.37	**0.42**
68%	EKF-ERTSS	0.15	0.12	**0.20**	0.14	0.11	**0.20**	0.14	0.10	**0.18**	0.14	0.12	**0.18**	0.22	0.20	**0.36**
	EKF	0.16	0.13	**0.22**	0.16	0.13	**0.22**	0.16	0.13	**0.23**	0.19	0.15	**0.27**	0.21	0.21	**0.37**
	LS-RTS	0.17	0.13	**0.21**	0.16	0.12	**0.20**	0.15	0.10	**0.18**	0.16	0.14	**0.22**	0.28	0.25	**0.39**
	LS	0.18	0.14	**0.23**	0.17	0.14	**0.23**	0.17	0.12	**0.23**	0.18	0.17	**0.25**	0.18	0.16	**0.23**
95%	EKF-ERTSS	0.31	0.27	**0.38**	0.27	0.24	**0.32**	0.28	0.25	**0.36**	0.29	0.20	**0.34**	0.43	0.47	**0.56**
	EKF	0.34	0.30	**0.41**	0.31	0.28	**0.38**	0.24	0.38	**0.42**	0.40	0.40	**0.59**	0.46	0.80	**0.97**
	LS-RTS	0.36	0.33	**0.51**	0.31	0.26	**0.36**	0.28	0.21	**0.33**	0.34	0.24	**0.34**	0.61	0.48	**0.62**
	LS	0.37	0.37	**0.52**	0.24	0.30	**0.40**	0.34	0.30	**0.40**	0.31	0.37	**0.41**	0.33	0.37	**0.41**
Number of the location points		831			398			216			84			51		

TABLE VI
TIME CONSUMPTION ON THE POSITIONING ESTIMATIONS, UNIT [SECONDS]

Item	Method	20 Hz*	10 Hz	5 Hz	2 Hz	1 Hz
Trajectory 1*	EKF-ERTSS	**0.69**	0.33	0.19	0.10	0.06
	EKF	**0.56**	0.29	0.16	0.08	0.05
	LS-RTS	**0.48**	0.25	0.14	0.07	0.04
	LS	**0.44**	0.23	0.13	0.06	0.04
Trajectory 2*	EKF-ERTSS	**3.10**	1.41	0.70	0.30	0.16
	EKF	**2.80**	1.24	0.60	0.26	0.14
	LS-RTS	**1.97**	1.01	0.54	0.23	0.12
	LS	**1.82**	0.91	0.47	0.20	0.11

*There are 6192 and 28763 location points within Trajectories 1 and 2 in total for the 20 Hz positioning update rate, respectively.

rate is also optimal. Thus, the processor will have enough time intervals for positioning processing.

In summary, all four positioning methods achieve decimeter-level positioning accuracy for different positioning update rates and are all sufficient for standalone UWB positioning inside forest canopy, and the EKF-based methods achieve better performance in terms of positioning accuracy and reliability than the LS-based methods but more time consumption. For applications with various demands, optimal positioning methods with optimal configurations need to be considered before implementation of the system to obtain optimal performance. For example, to locate a forester or map the tree stem in forests, a maximum positioning update rate of 5 Hz might be sufficient for these applications, and both EKF- and LS-based methods are suitable. However, to locate and track, for example, a UAV or other robotics inside the forest canopy, a 20 Hz or even higher positioning update rate is necessary to obtain precise and continuous positioning results. The results of this study provide a valuable reference not only for GNSS-denied forest environments but also for other positioning applications.

VI. MULTIUSER SCALABILITY

In this section, multiuser scalability of the standalone UWB positioning inside forest canopy is discussed. Usually, it is limited as interfering messages from different UWB terminals may interrupt the required message exchange in the SS-TWR [35] or other communications in the network. The classical TDMA scheme is promising to address this by dividing the time in superframes, as shown in [36]. For the standalone UWB positioning solution used in this study, it is easy to achieve the TDMA scheme for different UWB terminals due to the integration of the GNSS module into each terminal used for synchronization.

Fig. 14 shows the solution for the future to support a larger number of UWB terminals working simultaneously inside forest canopy. First, each UWB terminal receives the GNSS signals and synchronizes the local time of the terminal to the UTC time by capturing the PPS signals of the GNSS module. These terminals then autonomously determine their

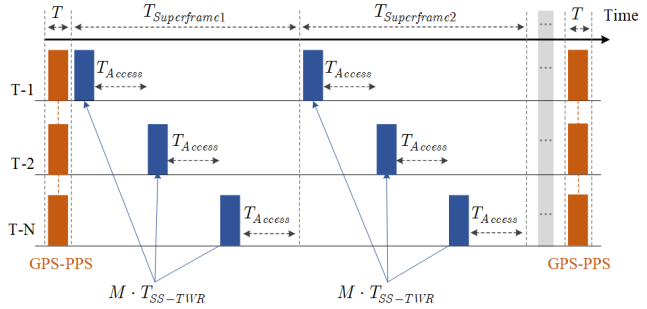

Fig. 14. Signal schedule for multiuser operation in the standalone UWB positioning inside forest canopy.

timestamps to start the SS-TWR based on the unique device ID in the network. Although the positioning accuracy of the GNSS is limited inside forest canopy, the PPS is accurately used to synchronize all the terminals in these environments. The synchronization accuracy highly depends on the resolution of the local time of the terminal and the threads executed in the processor. In this study, the UWB terminal achieved a synchronization accuracy of better than 0.1 ms, in which an STM32F4 processor with a 0.1-ms system ticker was integrated. Better accuracy can be achieved by using a higher performance processor.

In addition, a fixed and known protection interval, known as the contention access period, is also included for all the terminals to further enable the TDMA scheme, as shown in Fig. 14. According to [36], the maximum number of UWB terminals that the system can support can be obtained by

$$N = \frac{T_{\text{Superframe}}}{M \cdot T_{\text{SS-TWR}} + T_{\text{Aceess}}} \tag{11}$$

where $T_{\text{Superframe}}$ is the time duration of each superframe determined by the expected positioning update rate, $T_{\text{SS-TWR}}$ is the frame duration of each SS-TWR determined by the configuration of the UWB chip and the processing speed of the embedded processor integrated into the UWB device, T_{Access} is the time duration of the contention access period set to avoid the UWB signal interference between devices, and M is the number of anchors used to determine the location of the terminal. For actual applications, the values of these parameters need to be considered carefully and weighed between each other based on the demand of the application to achieve the optimal performance of the system.

VII. Conclusion

This article presents a detailed performance analysis of a standalone UWB positioning system in an actual GNSS-denied forest environment with slight/serious NLOS propagations in terms of positioning accuracies for different NLOS conditions and the effect of the positioning update date as well as the time consumption for different positioning methods based on real-world datasets. The results show that the standalone UWB positioning system is able to reduce the meter-level positioning accuracy of GNSS in these areas down to the decimeter level (better than 0.3 m in the *OXY* plane), which is sufficient resolution for forest surveys. In addition, the results also show that the LS-based methods achieve comparable performance with EKF-based positioning methods in slight NLOS conditions. However, more reliable performance was achieved by EKF-based positioning methods than LS-based positioning methods. All the results provide a valuable reference not only for positioning solutions for forestry automation but also for other location-based services.

In addition, although the positioning accuracy of the standalone UWB positioning in the *OXZ* plane is meter level and worse than that in the *OXY* plane, it can be improved by increasing beacons to the network geometry or using IMU-based fusion solutions. Thus, precise 3-D positioning might be achieved with UWB, which is sufficient for forest surveys, for example, providing precise positioning for a UAV to model the forest in 3-D. This topic is worthy of future investigation. Moreover, performing real-time positioning would be a significant feat to provide precise locations for a UAV or other applications with UWB.

Author Contributions

Zuoya Liu, Harri Kaartinen, Teemu Hakala, Juha Hyyppä, and Antero Kukko designed the concept of the method, and Zuoya Liu developed the method. The hardware platforms used in this article were created by Zuoya Liu and Teemu Hakala. The experimental design and data collection were performed by Zuoya Liu and Harri Kaartinen in the summer of 2023. Teemu Hakala and Harri Kaartinen provided other resources required for the experiment. The paper was mainly written by Zuoya Liu and reviewed and assisted by Harri Kaartinen, Teemu Hakala, Juha Hyyppä, Antero Kukko, and Ruizhi Chen. All authors contributed to the finalization of the manuscript and have read and agreed to the published version of the manuscript.

Declaration of Competing Interests

The authors declare that they have no known competing financial interests or personal relationships that could have appeared to influence the work reported in this article.

References

[1] E. Hyyppä et al., "Under-canopy UAV laser scanning for accurate forest field measurements," *ISPRS J. Photogramm. Remote Sens.*, vol. 164, pp. 41–60, Jun. 2020.

[2] A. Jaakkola et al., "Autonomous collection of forest field reference—The outlook and a first step with UAV laser scanning," *Remote Sens.*, vol. 9, no. 8, p. 785, Jul. 2017.

[3] A. Proudman, M. Ramezani, S. T. Digumarti, N. Chebrolu, and M. Fallon, "Towards real-time forest inventory using handheld LiDAR," *Robot. Auto. Syst.*, vol. 157, Nov. 2022, Art. no. 104240.

[4] R. Visser and O. F. Obi, "Automation and robotics in forest harvesting operations: Identifying near-term opportunities," *Croatian J. Forest Eng.*, vol. 42, no. 1, pp. 13–24, 2021.

[5] J. M. Dow, R. Neilan, and C. Rizos, "The international GNSS service in a changing landscape of global navigation satellite systems," *J. Geodesy*, vol. 83, nos. 3–4, pp. 191–198, Mar. 2009.

[6] J. C. J. Koelemeij, H. Dun, C. E. V. Diouf, E. F. Dierikx, G. J. M. Janssen, and C. C. J. M. Tiberius, "A hybrid optical–wireless network for decimetre-level terrestrial positioning," *Nature*, vol. 611, no. 7936, pp. 473–478, Nov. 2022.

[7] M. Bakuła, S. Oszczak, and R. Pelc-Mieczkowska, "Performance of RTK positioning in forest conditions: Case study," *J. Surveying Eng.*, vol. 135, no. 3, pp. 125–130, Aug. 2009.

[8] M. Perez-Ruiz, D. C. Slaughter, C. Gliever, and S. K. Upadhyaya, "Tractor-based real-time kinematic-global positioning system (RTK-GPS) guidance system for geospatial mapping of row crop transplant," *Biosystems Eng.*, vol. 111, no. 1, pp. 64–71, Jan. 2012.

[9] H. Kaartinen et al., "Accuracy of kinematic positioning using global satellite navigation systems under forest canopies," *Forests*, vol. 6, no. 9, pp. 3218–3236, Sep. 2015.

[10] D. Kai, O. Steve, J. Grzegorz, K. T. Charles, and A. G.-B. Dorota, "UWB for navigation in GNSS compromised environments," in *Proc. 28th Int. Tech. Meeting Satell. Division Inst. Navigat. (ION GNSS+)*, 2015, pp. 2380–2389.

[11] C. R. Anderson, H. I. Volos, and R. M. Buehrer, "Characterization of low-antenna ultrawideband propagation in a forest environment," *IEEE Trans. Veh. Technol.*, vol. 62, no. 7, pp. 2878–2895, Sep. 2013.

[12] T. Faitli, T. Hakala, H. Kaartinen, J. Hyyppä, and A. Kukko, "Real-time LiDAR-inertial positioning and mapping for forestry automation," *Int. Arch. Photogramm., Remote Sens. Spatial Inf. Sci.*, vol. XLVIII-1, pp. 145–150, May 2023.

[13] M. Pierzchala, P. Giguère, and R. Astrup, "Mapping forests using an unmanned ground vehicle with 3D LiDAR and graph-SLAM," *Comput. Electron. Agricult.*, vol. 145, pp. 217–225, Feb. 2018.

[14] A. Kukko, R. Kaijaluoto, H. Kaartinen, V. V. Lehtola, A. Jaakkola, and J. Hyyppä, "Graph SLAM correction for single scanner MLS forest data under boreal forest canopy," *ISPRS J. Photogramm. Remote Sens.*, vol. 132, pp. 199–209, Oct. 2017.

[15] X. Liang, H. Yao, H. Qi, and X. Wang, "Forest in situ observations through a fully automated under-canopy unmanned aerial vehicle," *GeoSpatial Inf. Sci.*, pp. 1–17, Mar. 2024.

[16] H. Nguyen, R. Andersen, E. Boukas, and K. Alexis, "Uncertainty-aware visually-attentive navigation using deep neural networks," *Int. J. Robot. Res.*, vol. 43, no. 6, pp. 840–872, May 2024.

[17] F. A. Ruetz, N. Lawrance, E. Hernández, P. V. K. Borges, and T. Peynot, "ForestTrav: 3D LiDAR-only forest traversability estimation for autonomous ground vehicles," *IEEE Access*, vol. 12, pp. 37192–37206, 2024.

[18] L. Flueratoru, S. Wehrli, M. Magno, E. S. Lohan, and D. Niculescu, "High-accuracy ranging and localization with ultrawideband communications for energy-constrained devices," *IEEE Internet Things J.*, vol. 9, no. 10, pp. 7463–7480, May 2022.

[19] *APS011: Application Note Sources of Error in DW1000 Based Two-Way Ranging (TWR) Schemes*, Decawave, Dublin, Ireland, 2014.

[20] A. Mussina and S. Aubakirov, "RSSI based Bluetooth low energy indoor positioning," in *Proc. IEEE 12th Int. Conf. Appl. Inf. Commun. Technol. (AICT)*, Oct. 2018, pp. 1–4.

[21] B. Zhou, Z. Wu, Z. Chen, X. Liu, and Q. Li, "Wi-Fi RTT/encoder/INS-based robot indoor localization using smartphones," *IEEE Trans. Veh. Technol.*, vol. 72, no. 5, pp. 6683–6694, May 2023.

[22] L. Chen, X. Zhou, F. Chen, L.-L. Yang, and R. Chen, "Carrier phase ranging for indoor positioning with 5G NR signals," *IEEE Internet Things J.*, vol. 9, no. 13, pp. 10908–10919, Jul. 2022.

[23] Wikipedia. *Ultra-Wideband*. Accessed: Jun. 2, 2024. [Online]. Available: https://en.wikipedia.org/wiki/Ultra-wideband

[24] A. Alarifi et al., "Ultra wideband indoor positioning technologies: Analysis and recent advances," *Sensors*, vol. 16, no. 5, p. 707, May 2016.

[25] A. R. J. Ruiz and F. S. Granja, "Comparing Ubisense, BeSpoon, and DecaWave UWB location systems: Indoor performance analysis," *IEEE Trans. Instrum. Meas.*, vol. 66, no. 8, pp. 2106–2117, Aug. 2017.

[26] J. Li, Y. Bi, K. Li, K. Wang, F. Lin, and B. M. Chen, "Accurate 3D localization for MAV swarms by UWB and IMU fusion," 2018, *arXiv:1807.10913*.

[27] A. Ledergerber and R. D. Andrea, "Ultra-wideband range measurement model with Gaussian processes," in *Proc. IEEE Conf. Control Technol. Appl. (CCTA)*, Aug. 2017, pp. 1929–1934.

[28] Z. Sahinoglu and I. Guvenc, "Threshold-based TOA estimation for impulse radio UWB systems," in *Proc. IEEE Int. Conf. Ultra-Wideband*, Sep. 2005, pp. 420–425.

[29] Z. Liu, T. Hakala, J. Hyyppä, A. Kukko, H. Kaartinen, and R. Chen, "Data-driven antenna delay calibration for UWB devices for network positioning," *IEEE Trans. Instrum. Meas.*, vol. 73, pp. 1–11, 2024.

[30] A. De Preter, G. Goysens, J. Anthonis, J. Swevers, and G. Pipeleers, "Range bias modeling and autocalibration of an UWB positioning system," in *Proc. Int. Conf. Indoor Positioning Indoor Navigat. (IPIN)*, Sep. 2019, pp. 1–8.

[31] J. Choliz, M. Eguizabal, A. Hernandez-Solana, and A. Valdovinos, "Comparison of algorithms for UWB indoor location and tracking systems," in *Proc. IEEE 73rd Veh. Technol. Conf. (VTC Spring)*, May 2011, pp. 1–5.

[32] S. Sarkka, *Bayesian Filtering and Smoothing*. Cambridge, U.K.: Cambridge Univ. Press, 2013.

[33] H. E. Rauch, F. Tung, and C. T. Striebel, "Maximum likelihood estimates of linear dynamic systems," *AIAA J.*, vol. 3, no. 8, pp. 1445–1450, 1965.

[34] D. Neirynck, E. Luk, and M. McLaughlin, "An alternative double-sided two-way ranging method," in *Proc. 13th Workshop Positioning, Navigat. Commun. (WPNC)*, Oct. 2016, pp. 1–4.

[35] J. Tiemann and C. Wietfeld, "Scalability, real-time capabilities, and energy efficiency in ultra-wideband localization," *IEEE Trans. Ind. Informat.*, vol. 15, no. 12, pp. 6313–6321, Dec. 2019.

[36] M. Ridolfi, S. Van De Velde, H. Steendam, and E. De Poorter, "Analysis of the scalability of UWB indoor localization solutions for high user densities," *Sensors*, vol. 18, no. 6, p. 1875, Jun. 2018.

Zuoya Liu is currently a Post-Doctoral Fellow with the Department of Remote Sensing and Photogrammetry, Finnish Geospatial Research Institute, Espoo, Finland. His research interests include positioning and navigation technologies, wireless networks, multisensor cooperative control, signal processing, the Internet of Things, and forest surveying.

Harri Kaartinen is currently a Research Professor with the Department of Remote Sensing and Photogrammetry, Finnish Geospatial Research Institute, Espoo, Finland. He coordinates and conducts research on performance and quality issues related to laser scanning sensors, systems, and applications, with abundant skills and expertise in GNSS, geomatic, laser scanning, mapping, and remote sensing.

Teemu Hakala is currently an Academic Researcher with the Department of Remote Sensing and Photogrammetry, Finnish Geospatial Research Institute, Espoo, Finland. He has contributed to research in topics: terrestrial, mobile and airborne laser scanning, spectrometry, hyperspectral imaging and LiDAR, drone, and forest health.

Juha Hyyppä is currently a Professor and the Director of the Department of Remote Sensing and Photogrammetry, Finnish Geospatial Research Institute, Espoo, Finland. His research interests include laser scanning systems, their performance, and new applications, especially related to mobile and ubiquitous laser scanning systems, including autonomous driving and point cloud processing.

Antero Kukko is currently a Professor with the Department of Remote Sensing and Photogrammetry, Finnish Geospatial Research Institute, Espoo, Finland. His expertise comprises a variety of aspects of laser scanning and image data, including both system developments and data processing for mobile and airborne laser scanning, and research and development of automatic image registration methods.

Ruizhi Chen is a Professor with the State Key Laboratory of Information Engineering in Surveying, Mapping and Remote Sensing, Wuhan University, Wuhan, China, where he is an Academician with the Finnish Academy of Science and Letters. He is committed to theoretical research and core technology development for seamless indoor/outdoor positioning using smartphones.